Chiral-induced angular momentum radiation in single molecular junctions

Bing-Zhong Hu,[1] Zu-Quan Zhang,[2] Lei-Lei Nian,[3] and Jing-Tao Lü[1, ∗]

[1]*School of Physics, Institute for Quantum Science and Engineering and Wuhan National High Magnetic Field Center, Huazhong University of Science and Technology, Wuhan 430074, People's Republic of China*

[2]*Department of Physics, Zhejiang Normal University, Jinhua 321004, People's Republic of China*

[3]*School of Physics and Astronomy, Yunnan University, Kunming 650091, People's Republic of China*

(Dated: March 22, 2023)

Abstract

We study angular momentum radiation from electrically-biased chiral single molecular junctions using the nonequilibrium Green's function method. Using single and double helical chains as examples, we make connections between the ability of a chiral molecule to emit photons with angular momentum to the geometrical factors of the molecule. We point out that the mechanism studied here does not involve the magnetic dipole momentum. Rather, it relies on inelastic transitions between scattering states originated from two electrodes with different chiral properties and chemical potentials. Thus, the required time-reversal symmetry breaking is provided by nonequilibrium electron transport.

I. INTRODUCTION

Angular momentum(AM) is a fundamental property of light[1–6], whose generation and manipulation is of vital importance for their applications in optoelectronics, quantum information science, and so on[6–10]. Light with AM can be generated by physical objects with vastly different scales, from as small as synchrotron in particle physics[11–14] to as large as rotating black hole in astrophysics[15]. The AM of light can be furthermore used to probe the spin-polarized electronic structure and to study other types of chiral excitations.

The magneto-electric coupling, depending on both the magnetic and electric dipole transition elements, is a key factor that determines the magnitude or efficiency of many of the above-mentioned processes[16]. Unfortunately, the magnetic dipole transition is much weaker than the corresponding electric one, resulting in a small magneto-electric coupling. Employing the chiral geometric or electronic structure in electric dipole transitions is a promising approach to avoid the weak magnetic dipole transition, given that the time-reversal symmetry breaking is provided by other mechanisms. Recently, it has been shown theoretically that coupling of electron orbital motion with light in current-carrying molecular junctions can lead to AM radiation (AMR)[17–21]. Electroluminescence from single molecules or localized gap plasmons in a scanning tunneling microscope (STM) has been studied for decades [22–28]. Different quantum statistical properties of emitted light has

---

* jtlu@hust.edu.cn

been characterized using STM setup[29–33]. Thus, it is also an ideal experimental candidate to study AMR at the single molecular scale.

On the other hand, molecular electronics and optoelectronics using chiral molecules such as DNA have been the focus of recent intense research[34]. In the phenomenon of chiral-induced spin selectivity (CISS)[35–41], spin-polarized electrons can be generated from chiral molecular structure driven by electrical or optical stimuli. Spin-orbit interaction is argued to play an important role, although the exact mechanism is still under debate. In light emitting diode, large chiroptical effects are observed from chiral molecular structures[39, 42]. It origin is attributed to either the magneto-electric coupling (natural optical activity), or structural chirality. Notably, a recent work proposed an electronic mechanism employing the topological electronic structure for circular polarized light emission under electrical current flow[43]. The common trends of CISS and optical dichroism in helical structures is also studied very recently[41].

In this work, we study theoretically AMR from junctions of model helical chains using nonequilibrium Green's function (NEGF) method[17, 44]. We analyze in details how the molecular geometry, electronic structure and molecule-electrode coupling influence the spectrum and efficiency of AMR. Suitable conditions for enhancing the AMR are proposed based on the numerical calculation.

II.   MODEL AND THEORY

A.   Hamiltonian

We use a tight binding model to write the Hamiltonian of the molecule as [17, 18]

$$H_{\text{mol}} = \sum_{ij} H_{ij} c_i^\dagger c_j e^{i\theta_{ij}}. \tag{1}$$

Molecular coupling to the radiation fields is taken into account by the Peierls substitution[45] with the phase factor θ_{ij} between sites i and j

$$\theta_{ij} = \frac{e}{\hbar} \int_{r_j}^{r_i} \boldsymbol{A} \cdot d\boldsymbol{l}. \tag{2}$$

3

Here e is the elementary charge, $\hbar$ is the reduced Planck constant, and $\boldsymbol{A}$ is the vector potential of the electromagnetic field, which is described by the following Hamiltonian

$$H_{\text{rad}} = \frac{1}{2} \int d^3 \boldsymbol{r} \left(\varepsilon_0 \boldsymbol{E}_\perp^2 + \frac{1}{\mu_0} \boldsymbol{B}^2 \right), \tag{3}$$

where ε_0, μ_0 the vacuum permittivity and permeability, respectively. $\boldsymbol{E}_\perp$ and $\boldsymbol{B}$ are electric field and magnetic field in the transverse gauge $\nabla \cdot \boldsymbol{A} = 0$. They are written in terms of $\boldsymbol{A}$ as $\boldsymbol{E}_\perp = -\partial_t \boldsymbol{A}$, $\boldsymbol{B} = \nabla \times \boldsymbol{A}$. By expanding the exponential part to the first order in $\boldsymbol{A}$, we can divide the molecule Hamiltonian into two terms

$$H_{\text{mol}} = H_0 + H_{\text{int}}.$$

The first term H_0 is the non-interacting part

$$H_0 = \sum_{i,j} H_{ij} c_i^\dagger c_j, \tag{4}$$

and H_{int} is the interacting part

$$H_{int} \approx \sum_{ij} \sum_k \sum_{\mu=x,y,z} M_{ij}^{k\mu} c_i^\dagger c_j A_\mu \left(\boldsymbol{r}_k \right),$$
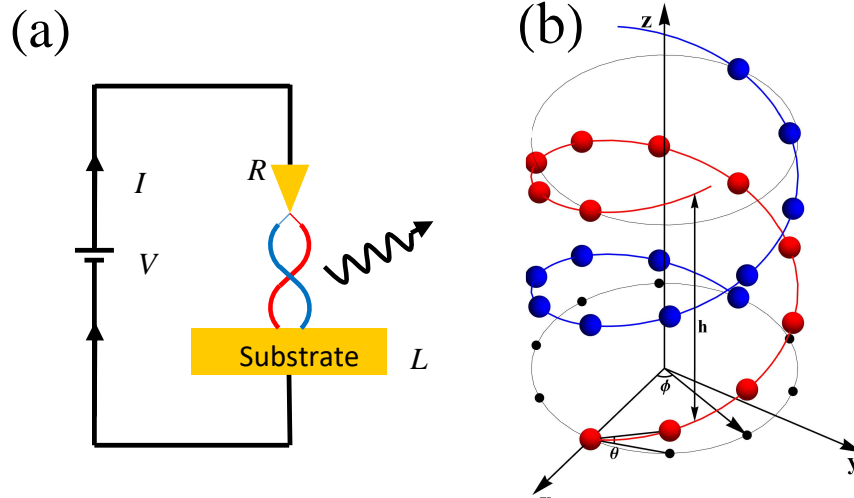

FIG. 1. (a) Schematic diagram of angular momentum radiation from voltage-biased chiral molecule. (b) A double helical chain structure with radius R, pitch h, helix angle θ, and arc length l_a.

4

where

$$M_{ij}^{k\mu} = \frac{ie}{2\hbar} H_{ij} \left(\boldsymbol{r}_i - \boldsymbol{r}_j \right)_\mu \left(\delta_{ki} + \delta_{kj} \right)$$

is electron-photon coupling matrix.

As an example, the noninteracting molecular Hamiltonian for a double helical chain simulating double-stranded DNA is

$$H_{0,\text{ds}} = \sum_{j=1}^{2} \left[\sum_{n=1}^{N} \varepsilon_{jn} c_{jn}^\dagger c_{jn} + \sum_{n,m} \left(t_j c_{jn}^\dagger c_{jm} + \text{ h.c. } \right) \right] + \sum_{n=1}^{N} \left(t_n^{IC} c_{1n}^\dagger c_{2n} + \text{ h.c. } \right). \quad (5)$$

Here, j is the chain index, and m, n are site indices, ε_{jn} is onsite energy of site n in chain j, $t_{j,nm}$ is inter-site hopping within chain j, t_n^{IC} is inter-chain hopping, c_{jn} ($c_{jn}^\dagger$) is annihilation (creation) operator of electron at site n in chain j. This Hamiltonian has been used in previous works to study spin-dependent electron transport in ds-DNA [46, 47]. For single helical chain, we can simply set $j = 1$ and drop the inter-chain hopping term. Note that we have ignored the spin-orbit coupling in this work. We have checked that it does not bring any new physical effect, contrary to the CISS effect.

To consider electron transport process, we take into account the molecule-electrode coupling in the wide band limit. Two characteristic quantity Γ_L and Γ_R are used to model its coupling to the left and right electrodes, respectively. We make further simplification to write Γ_α as a diagonal matrix, whose non-zero diagonal elements are of the same magnitude γ_α. The positions of the non-zero diagonals are determined by the way how the molecule couples to the electrode, i.e., all the degrees of freedom that couple directly to electrode has a non-zero element, and the rest elements are zero.

B. Light and angular momentum radiation

By applying the non-equilibrium Green's function (NEGF) method, we can calculate various physical quantities such as electrical current, light and angular momentum radiation, and so on. The radiated power P, angular momentum flux J_γ and the photon flux J_N can then be written in terms of the self-energy[17, 48]

$$P = \frac{dW}{dt} = -\sum_\mu \int_0^\infty \frac{d\omega}{2\pi} \frac{\hbar\omega^2}{3\pi\varepsilon_0 c^3} \text{Im} \left[\Pi_{\mu\mu}^{\text{tot},<}(\omega) \right], \quad (6)$$

$$J_\gamma = \frac{dL_\gamma}{dt} = \int_0^\infty \frac{d\omega}{2\pi} \frac{\hbar\omega}{3\pi\varepsilon_0 c^3} \epsilon_{\gamma\mu\nu} \text{Re} \left[\Pi_{\mu\nu}^{\text{tot},<}(\omega) \right], \quad (7)$$

5

$$J_N = \frac{dN}{dt} = -\sum_{\mu} \int_0^\infty \frac{d\omega}{2\pi} \frac{\omega}{3\pi\varepsilon_0 c^3} \, \text{Im} \left[\Pi_{\mu\mu}^{\text{tot},<}(\omega) \right]. \tag{8}$$

Here, μ, ν and γ are indices for the Cartesian coordinate, ε_0, c and $\hbar$ are the vacuum permittivity, the speed of light in the vacuum, and the reduced Planck constant, respectively. The superscript 'tot' means summation over all the sites in the system $\Pi_{\mu\nu}^{\text{tot},<}(\omega) = \sum_{i,j} \Pi_{\mu\nu}^<(\boldsymbol{r}_i, \boldsymbol{r}_j, \omega)$, where $\Pi_{\mu\nu}^<$ is photon self-energy due to interaction with electrons.

Under the random phase approximation, the photon self-energy is written as

$$\Pi_{\mu\nu}^<(\boldsymbol{r}_i, \boldsymbol{r}_j, \omega) = -i\hbar \int_{-\infty}^\infty \frac{dE}{2\pi\hbar} \, \text{Tr} \left[M^{i\mu} G^<(E) M^{j\nu} G^>(E - \hbar\omega) \right] \tag{9}$$

Here, $\text{Tr}[...]$ is trace over all electronic degrees of freedom. The greater/lesser Green's function of non-interacting electrons is given by $G^{>/<}(E) = G^r(E)\Sigma^{>/<}(E)G^a(E)$, with $\Sigma^{>/<}(E) = \Sigma_L^{>/<}(E) + \Sigma_R^{>/<}(E)$ the greater/lesser self-energy due to electron coupling to left and right electrodes, and $E^- = E - \hbar\omega$. In the wide band limit, the self-energy is energy independent $\Sigma_\alpha^r = -i\Gamma_\alpha/2$.

For the ease of analysis, we define

$$X_{\mu\nu}^{\alpha\beta}(E, E^-) = \text{Tr} \left[V^\mu A^\alpha(E) V^\nu A^\beta(E^-) \right] \tag{10}$$

$$= 2\pi \sum_{m,n} \langle \psi_{\alpha,m}(E)|V^\nu|\psi_{\beta,n}(E^-)\rangle \langle \psi_{\beta,n}(E^-)|V^\mu|\psi_{\alpha,m}(E)\rangle. \tag{11}$$

where $A^\alpha(E) = G^r(E)\Gamma^\alpha(E)G^a(E)$ is spectral function contributed by scattering states from electrode α, V^μ is electron velocity matrix $V^\mu = \frac{1}{ie} \sum_k M^{k\mu}$, with $V_{ij}^\mu = H_{ij}(r_i^\mu - r_j^\mu)/\hbar$. In the second equation, we have written it in terms of velocity matrix elements between scattering states. This form highlights the origin of AMR as inelastic transitions from scattering states of one electrode to those of the other. We can show that the following relations hold: (i) $X_{\mu\nu}^{\alpha\beta}(E, E^-) = X_{\nu\mu}^{\beta\alpha}(E^-, E)$, (ii) $X_{\mu\nu}^{\alpha\beta}(E, E^-) = [X_{\nu\mu}^{\alpha\beta}(E, E^-)]^*$. The photon less self-energy in the zero temperature limit can then be written as

$$\Pi_{\mu\nu}^{\text{tot},<}(\omega) = -ie^2\hbar \sum_{\alpha,\beta=L,R} \int_{\mu_\beta + \hbar\omega}^{\mu_\alpha} \frac{dE}{2\pi\hbar} \Theta(\mu_\alpha - \mu_\beta - \hbar\omega)$$

$$\times X_{\mu\nu}^{\alpha\beta}(E, E^-)(f^\alpha(E) - f^\beta(E^-)) \tag{12}$$

Here, $f^\alpha(E) = 1/(\exp((E - \mu_\alpha)/k_B T) + 1)$ is the Fermi-Dirac distribution function of electrode α, and $\Theta(E)$ is the Heaviside step function, which gives the energy range where the

inelastic transitions can take place. We focus on AMR along z direction in the case of $eV = \mu_L - \mu_R > 0$. Writing $J_A = J_z$, we get

$$
\begin{aligned}
J_A &= \int_0^\infty d\omega \, J_A(\omega) \\
&= \frac{4\alpha}{3\pi c^2} \int_0^\infty \frac{d\hbar\omega}{2\pi} \omega \Theta(eV - \hbar\omega) \int_{\mu_R + \hbar\omega}^{\mu_L} \frac{dE}{2\pi} j_A(E, E^-)
\end{aligned}
\tag{13}
$$

with fine-structure constant $\alpha = e^2/(4\pi\varepsilon_0\hbar c) \approx 1/137$ and AMR contribution

$$
j_A(E, E^-) = 2\hbar \, \mathrm{Im} \, X_{xy}^{LR}(E, E^-).
\tag{14}
$$

Similarly,

$$
J_N = \frac{4\alpha}{3\pi c^2} \int_0^\infty \frac{d\hbar\omega}{2\pi} \omega \Theta(\mu_L - \mu_R - \hbar\omega) \int_{\mu_R + \hbar\omega}^{\mu_L} \frac{dE}{2\pi} j_N(E, E^-)
\tag{15}
$$

with

$$
j_N(E, E^-) = \mathrm{Re} \left\{ X_{xx}^{LR}(E, E^-) + X_{yy}^{LR}(E, E^-) + X_{zz}^{LR}(E, E^-) \right\}.
\tag{16}
$$

We will apply the above theory to helical chain structures to study how the AMR depends on the molecule parameters and its coupling to the electrodes.

III.   RESULTS

A.   Angular momentum radiation spectra

We now present numerical results for model helical chain structures. We perform dimensionless calculation with $\hbar = e = l_a = t = 1$. The default parameters are following: the system temperature $T_L = T_R = 0$, the chemical potential $\mu_L = 4t, \mu_R = -4t$,the coupling larameter $\gamma_L = \gamma_R = 0.5$ t, radius of the chain $r_g = 7$ Å, arc length $l_a = 5.6$ Å, helix angle $\theta \approx 0.66$, and phase angle $\Delta\phi = \pi/5$. The electronic structure is modeled by using tight-binding parameters, with onsite energy set to zero, the nearest neighbour (NN) hopping $t_{\mathrm{NN}} = t$, different values of the next nearest neighbour (NNN) hopping t_{NNN} will be used. An energy step of $10^{-4}t$ is used to do the numerical integration, and the energy range is set to $[-5t, 5t]$.

We start from the simplest structure of a single helical chain with length $N = 3$. The AMR can be analyzed through the energy dependence of $j_A(E, E^-)$. From Eq. (13) we see

that the emission spectrum of the system at given energy $\hbar\omega$ can be obtained by integrating along a line cut over an effective bias window where the inelastic optical transition can take place. This bias window is determined by the relative positions between the two electrode chemical potentials, controlled by the Θ function in Eq. (13). Thus, $j_A(E, E^-)$ can be used to characterize the ability of the system to emit radiation with angular momentum. This is especially useful in molecular junctions where the rotational symmetry is broken and orbital angular momentum can no longer be used to characterize the symmetry property of molecular orbitals, as in simple molecules[17]. The total AMR is obtained by integrating j_A over E and ω. Figure 2 summarizes the main results with NN (upper row) and NNN (lower row) hopping, respectively. We can identify several noteworthy points:

- Sharp peaks are observed and dominate the contribution in the parameter space (E, E^-). Their positions correspond to $\hbar\omega = E_{32} = E_{21}$ [Fig. 2(d)]. The positive and negative values correspond to opposite angular momentum radiation, i.e., inelastic transition from state 3 to 2 and from 2 to 1 in Fig. 2(d) contributes oppositely.

- Switching electron and hole energy, j_A remains unchanged. This can be shown analytically (Appendix A) and is reflected by the symmetry about line $E = E^-$. For a given photon energy $\hbar\omega$, the integral in Eq. (13) over E is along a line (red dashed line for example). j_A is odd about the point where this line crosses with line $E + E^- = 0$. Inclusion of NNN hopping breaks the second symmetry, while keeping the first intact.

- Inelastic transition from state 3 to 1 can not generate AMR in the NN case. But this 'selection rule' is broken once NNN is included.

- According to these symmetries, in the large bias limit $\mu_L \gg E_n \gg \mu_R$, the total AMR is zero. However, if it is possible to include only part of the region, AMR becomes possible. In realistic structure, this may be achieved by: (1) selective enhancement of certain spectral range, i.e., via localized gap plasmon modes in a junction[32, 49], (2) electrical tuning of molecular levels through gating or source-drain voltage in a transistor setup.

To make the system more realistic, we increase the chain length to $N = 10$. The AMR distribution represented by $j_A(E, E^-)$ spreads to much larger regions (Fig. 3). The effect of NNN hopping on angular momentum radiation is more dramatic than the shorter chain. The
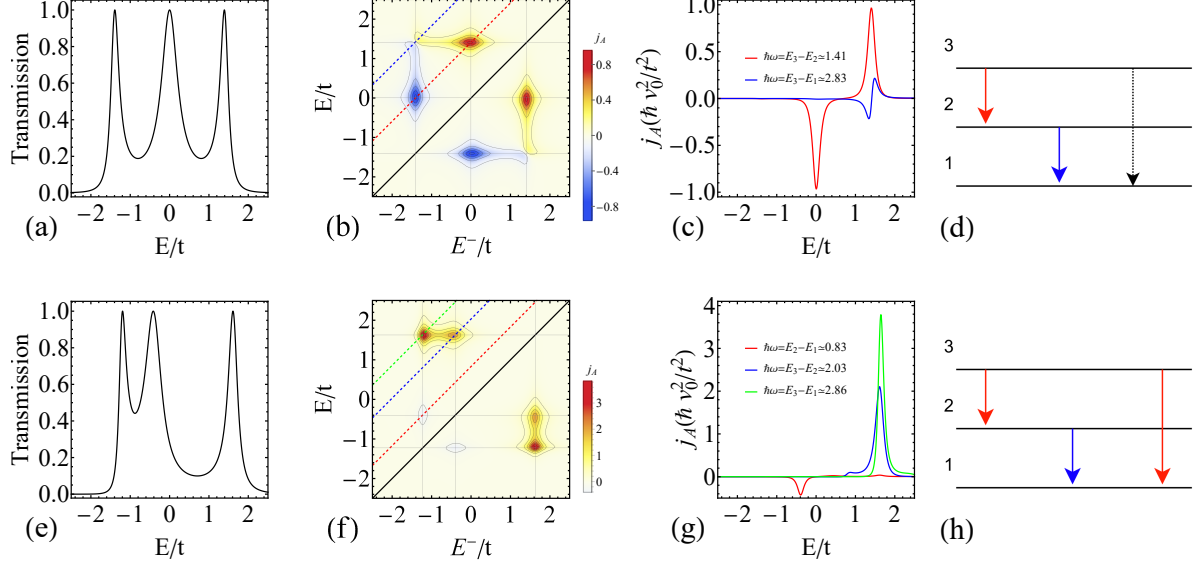
FIG. 2. Numerical results for a single helical chain with $N = 3$. In the upper row, only the nearest neighbour (NN) hopping $t_{NN} = t$ is included. In the lower row, in additional to t_{NN}, next nearest neighbour (NNN) hopping $t_{NNN} = 0.4t$ is included. (a, e) Electron transmission spectrum. (b, f) j_A as a function of energy E and E^- within the range [-2.5t,2.5t] . The velocity is $v_0 = l_a t/\hbar$. (c, g) Line cuts of the plot in (b, f). (d, h) IET Diagram. Red (blue) arrow represents transition with positive (negative) AMR, while dashed arrow corresponds to zero AMR.

negative regions shrink and the whole distribution is dominated by the positive regions. This is also reflected in the asymmetric distribution of the electron transmission in the positive and negative energy range. We have shown in Fig. 4 the dependence of J_A on the NNN hopping in the full bias regime, where the bias window encloses all the molecular orbitals. We observe increase of both magnitude and efficiency of AMR, and the efficiency J_A/J_N saturates at around $0.3\hbar$.

B. Geometrical dependence

To show the geometrical origin of the AMR in chiral molecules, dependence of AMR in the high bias limit on phase angle $\Delta\phi$ is shown in Fig. 5. It can be seen that AMR increases with the absolute value of phase angle. It is exactly zero (Appendix A) for achiral straight chain and changes sign when $\Delta\phi$ goes from positive to negative. Further analysis of
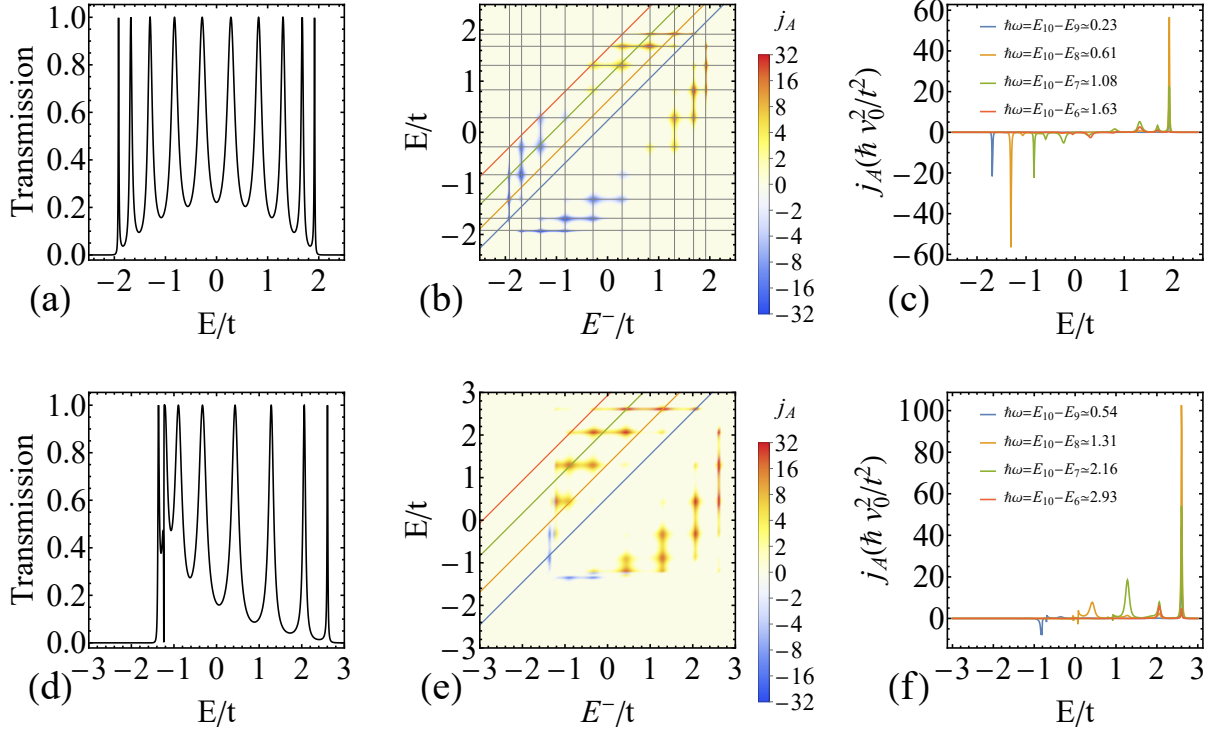
9

FIG. 3. Results for single helical chain with $N = 10$. Results with NN hopping are shown in the upper row (a-c). NNN hopping of $t_{\text{NNN}} = 0.4t$ is included for results shown in the lower row (d-f). (a, d) Electron transmission spectrum. (b, e) 2D plot of j_A as a function of energy E and E^-. Grid lines represent the eigen energy levels. (c, f) Line cut of the plot in (b, e) for different $\hbar\omega$, blue for 0.23, orange for 0.61, green for 1.08, red for 1.63.

$j_A(E, E^-)$ shows that the whole distribution in energy space reverses sign when $\Delta\phi$ changes sign. This positive correlation between AMR and chirality of the chain is one evidence of geometrical origin of AMR studied here.

We depict the length (N) and radius (R) dependence of the AMR in Fig. 6. We have integrated all the positive (termed Right-handed (RH), j_{AR}) and negative (termed Left-handed (LH), j_{AL}) regions of j_A in the energy space to characterize the system's ability to radiate angular momentum. When $\lambda = 0$, corresponding to zero NNN hopping, the positive and negative regions are of the same magnitude. They become asymmetric with enhanced positive AMR once $\lambda \neq 0$. In any case, the AMR grows linearly with chain length N and quadratically with radius R. This is the second evidence of geometrical nature of AMR.
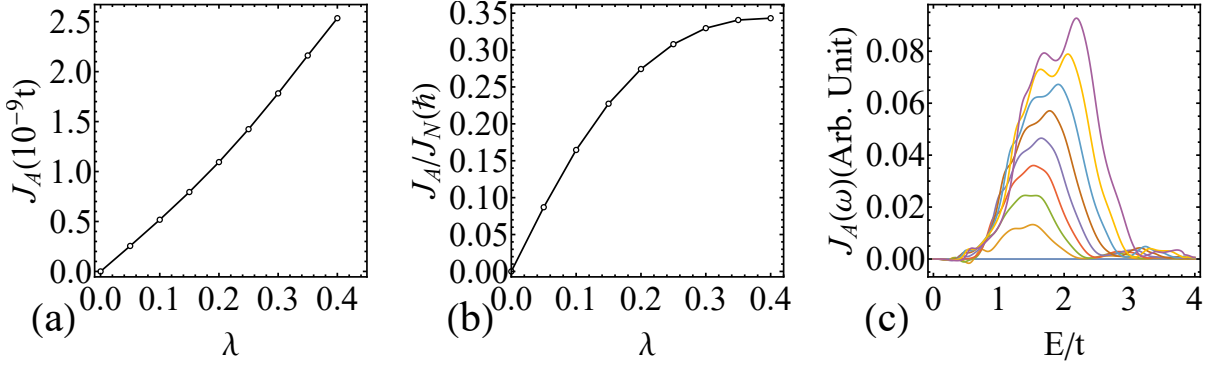
FIG. 4. AMR J_A (a), AMR per photon J_A/J_N (b) for single helical chain with $N = 10$ as a function of $\lambda = t_{\mathrm{NNN}}/t_{\mathrm{NN}}$ in the full bias case $\mu_L > \max\{\varepsilon_i\} > \min\{\varepsilon_i\} > \mu_R$, with $\{\varepsilon_i\}$ the set of eigen energies of the molecular orbitals. (c) AMR spectrum $J_A(\omega)$ from $\lambda = 0$ (bottom) to 0.4 (top).
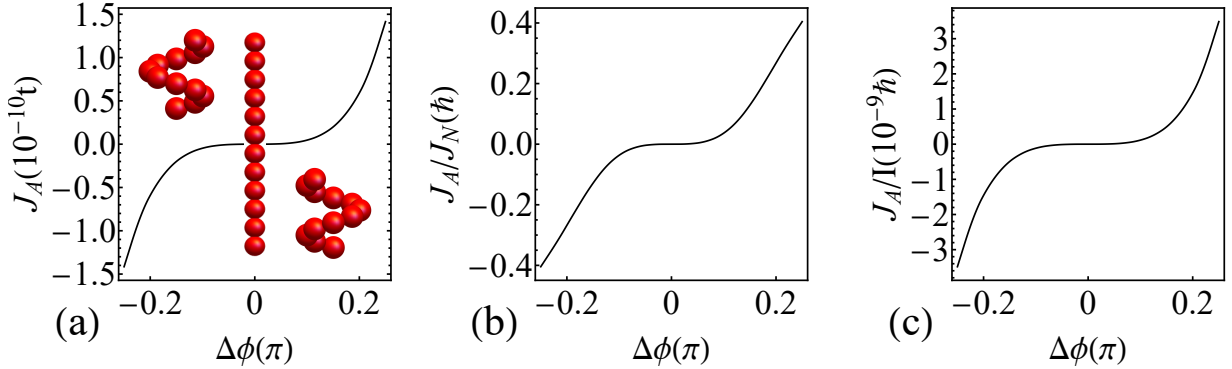

FIG. 5. Dependence of J_A (a), AMR per photon J_A/J_N (b) , AMR per electron J_A/J_E (c) as a function of phase angle $\Delta\phi$ for parameters $t_{\mathrm{NN}} = t, \lambda = 0.2, N = 12, \gamma_L = \gamma_R = 0.1t, \mu_L = 2t, \mu_R = -2t$. I is the current through the molecule. Insets of (a) show single helical chains with phase angle $\Delta\phi = -\pi/4, 0, \pi/4$, respectively.

C. Double-helical chain

Double-stranded DNA is a typical chiral molecule that has received considerable attention in molecular electronics[46, 50, 51]. We now use a commonly adopted tight-binding model of double helical chain to study its AMR property. Specifically, we take the following model parameters that resemble DNA[52]: NN hopping $t_{\mathrm{NN}} = 1.0$ eV, inter-chain hopping $t_{IC} = 2.4$
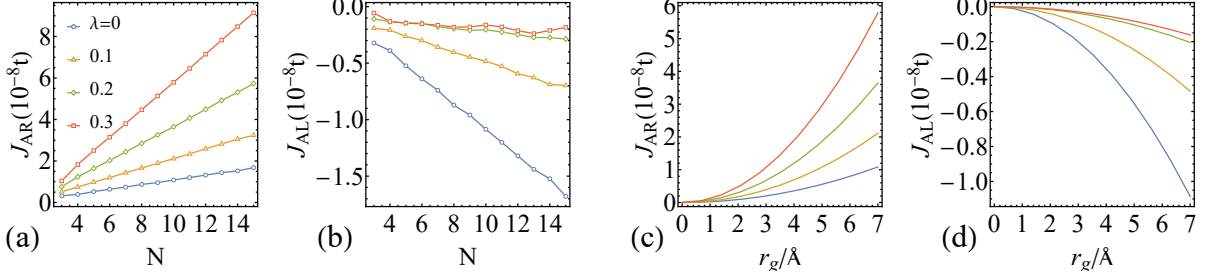
11

FIG. 6. Angular momentum radiation as a function of chain length N (a-b) and radius of gyration r_g (c-d) with different λ in the full bias regime. Default values are used for other parameters. J_{AR}: RH radiation corresponding to $j_A > 0$, J_{AL}: LH radiation corresponding to $j_A < 0$. Note the different scales of J_{AR} and J_{AL}.

eV, onsite energy $\varepsilon_{1,2} = \pm 0.56$ eV, NNN hopping $t_{\mathrm{NNN}} = 0$ eV, electrode coupling $\Gamma = 0.5$ eV.

We focus on the coupling of the molecule to the two electrodes, by consider two types of coupling [(I), (II) in Fig.7]. The first type is coherent coupling (I), whose 'off-diagonal' elements are non-zero

$$\Gamma_{ij}^L = \Gamma(\delta_{i1} + \delta_{i,N+1})(\delta_{j1} + \delta_{j,N+1}), \tag{17}$$

$$\Gamma_{ij}^R = \Gamma(\delta_{iN} + \delta_{i,2N})(\delta_{jN} + \delta_{j,2N}). \tag{18}$$

This introduces coherent coupling between the two chains. The second type is the incoherent type (II) with zero 'off-diagonal' elements

$$\Gamma_{ij}^{L,inco} = \Gamma(\delta_{i1} + \delta_{i,N+1})\delta_{ij}, \tag{19}$$

$$\Gamma_{ij}^{R,inco} = \Gamma(\delta_{iN} + \delta_{i,2N})\delta_{ij}. \tag{20}$$

In this case, electron transport and light emission processes are independent for the two chains. The final result is simply sum of contributions from each single helical chain.

The final results are summarized in Fig. 7. The first column compares electron transmission spectra for the two types of coupling to the electrodes. For coherent/incoherent coupling, the electron-hole pair symmetry in the transmission is broken/preserved. This has important consequence on photon and AMR spectra shown in the following columns. For incoherent coupling, j_A is anti-symmetric along diagonal lines $E = -E^-$. Integration over E and E^- leads to cancellation of contributions from opposite sides of the $E = -E^-$ line. This
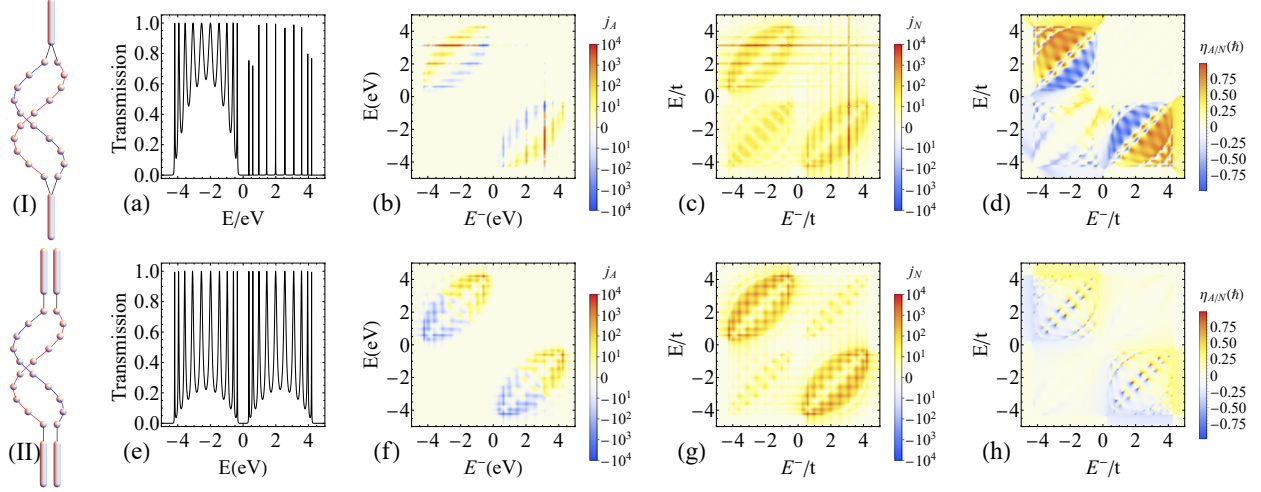
FIG. 7. Results for the double-helical chain with coherent (I, upper) and incoherent (II, lower) coupling to the two electrodes. (I, II) Schematic views of two types of coupling of the double helical chain to electrodes. (a-d) Electron transmission spectrum (a), 2D Plot of j_A (b), j_N (c) and $\eta^{A/N} = j_A/j_N$ (d) as a function of E and E^-, respectively. (e-h) The same as (a-d) but for incoherent coupling to electrodes.

can be avoided in the coherent coupling case due to the breaking of electron-hole symmetry. The resulting AMR efficiency $\eta_{A/N} = j_A/j_N$ is enhanced in a wide range of (E, E^-) space.

IV. DISCUSSIONS

We can try to understand these numerical results using Eqs. (11) nad (14). We see that the AMR in z direction is proportional to the imaginary part of the two electric dipole matrix elements in the x and y directions. Geometrical chiral properties of the molecule are encoded in the velocity matrix $V^\mu, \mu = x, y$. Both of them involve occupied scattering state from one electrode and unoccupied state from the other. Importantly, it does not involve any magnetic dipole matrix element. This is in contrast to circular dichroism and optical rotation in chiral molecules, where the magnetic dipole transition is critical[16]. Non-zero AMR needs breaking of time-reversal symmetry (TRS). In optical rotation and circular dichroism, the molecular eigen states are time-reversal symmetric. Breaking of TRS is realized by the external magnetic field. Meanwhile, the biased chiral molecular junction studied here is an open system. The electronic states participating the inelastic transition

are scattering states. The involved scattering states are determined by current direction. TRS breaking is realized by external bias and resulting electrical current. Thus, magnetic dipole transition is not necessary. This is the central observation of present study. It enables electrical generation of optical angular momentum utilizing the chiral geometric properties of the molecule without introducing magnetic field. It also differs from other approaches where optical angular momentum is generated by chiral wave guide from initially linear polarized light.

V. CONCLUSION

In summary, we have studied electrically driven AMR from helical chains using the nonequilibrium Green's function method. The ability of AMR is characterized by the imaginary part of a joint optical transition matrix element between scattering states originated from the two electrodes [Eq. (11)]. We have made direct connection between the geometrical factors and the radiation properties. The most important property of this chiral-induced AMR is that it does not rely on the magnetic dipole transition moment, which is normally much smaller compared to the electric counterpart and hinders the radiation efficiency. Rather, the mechanism studied here relies on the electrical dipole transitions at two different directions, from filled to empty scattering states originated from two different electrodes. We have also shown the dependence of AMR on the tight-binding parameters and the coupling to electrodes. These parameters allow electrical engineering of molecule's AMR property.

Appendix A: Properties for X

In this section, we derive the properties for X in Eq. (11) in the main text. Using the cyclic property of the trace, we get

$$X_{\mu\nu}^{\alpha\beta}(E, E^-) = \text{Tr}[V^\mu A^\alpha(E)V^\nu A^\beta(E^-)] = \text{Tr}[V^\nu A^\beta(E^-)V^\mu A^\alpha(E)] = X_{\nu\mu}^{\beta\alpha}(E^-, E) \quad (A1)$$

By noting that A^α, V^μ are Hermitian, we obtain another relationship by performing conjugate of X

$$X_{\mu\nu}^{\alpha\beta}(E, E^-) = \text{Tr}[V^\mu A^\alpha V^\nu A^{\beta-}] = \text{Tr}[V^\nu A^\alpha V^\mu A^{\beta-}]^* = [X_{\nu\mu}^{\alpha\beta}(E, E^-)]^* \quad (A2)$$

We use the above two equations and derive useful properties for X, which can help us to understand the results in the main text.

1. Single helical chain with NN hopping

The system under this case obeys particle-hole symmetry, from which we get one additional condition

$$g^r(-E) = g^a(E) \quad (A3)$$

In a physical sense, this means a process involving an energy E and a time-reversed process involving an energy $-E$ are equivalent. Similarly, The spectral function is also symmetric

$$A^{\alpha\top}(E) = -A^\alpha(-E). \quad (A4)$$

The above results lead to

$$\begin{aligned}
X_{xy}^{LR}(-E^-, -E) &= \text{Tr}[V^x A^L(-E^-)V^y A^R(-E)] \\
&= \text{Tr}[V^x A^{L\top}(E^-)V^y A^{R\top}(E)] \\
&= \text{Tr}[V^x A^R(E)V^y A^L(E^-)] \\
&= X_{xy}^{RL}(E, E^-)
\end{aligned} \quad (A5)$$

This means that for any transition $E \to E^-$, the AMR contribution is exactly the opposite of the corresponding transition $-E^- \to -E$. If both transitions are allowed in the large bias limit, their AMR contribution cancels.

2. Analysis of AMR for straight chain

For straight chain, r_{ij}^x / r_{ij}^y is constant, so is V^x/V^y. That means V^x and V^y are switchable by multiplying a constant. Then, we have $X_{xy}^{LR} = X_{yx}^{LR}$. Combining with Eq. (A2), we get

$$X_{xy}^{LR} = (X_{yx}^{LR})^* = X_{yx}^{LR} \tag{A6}$$

So $\mathrm{Im} X_{xy}^{LR} = 0$, meaning that AMR contribution j_A is zero for straight chain.

---

[1] J. H. Poynting, Proc. R. Soc. London, Ser. A **82**, 560 (1909).

[2] R. A. Beth, Phys. Rev. **50**, 115 (1936).

[3] P. Coullet, L. Gil, and F. Rocca, Opt. Commun. **73**, 403 (1989).

[4] L. Allen, M. W. Beijersbergen, R. J. C. Spreeuw, and J. P. Woerdman, Phys. Rev. A **45**, 8185 (1992).

[5] K. Y. Bliokh and F. Nori, Phys. Rep. **592**, 1 (2015).

[6] Y. Shen, X. Wang, Z. Xie, C. Min, X. Fu, Q. Liu, M. Gong, and X. Yuan, Light: Sci. Appl. **8**, 1 (2019).

[7] B. Jack, J. Leach, J. Romero, S. Franke-Arnold, M. Ritsch-Marte, S. M. Barnett, and M. J. Padgett, Phys. Rev. Lett. **103**, 083602 (2009).

[8] N. Bozinovic, Y. Yue, Y. Ren, M. Tur, P. Kristensen, H. Huang, A. E. Willner, and S. Ramachandran, Science **340**, 1545 (2013).

[9] D. L. Andrews, L. C. D. Romero, and M. Babiker, Opt. Commun. **237**, 133 (2004).

[10] M. Krenn, M. Huber, R. Fickler, R. Lapkiewicz, S. Ramelow, and A. Zeilinger, Proc. Natl. Acad. Sci. U.S.A. **111**, 6243 (2014).

[11] M. Katoh, M. Fujimoto, N. S. Mirian, T. Konomi, Y. Taira, T. Kaneyasu, M. Hosaka, N. Yamamoto, A. Mochihashi, Y. Takashima, K. Kuroda, A. Miyamoto, K. Miyamoto, and S. Sasaki, Sci. Rep. **7**, 6130 (2017).

[12] M. Katoh, M. Fujimoto, H. Kawaguchi, K. Tsuchiya, K. Ohmi, T. Kaneyasu, Y. Taira, M. Hosaka, A. Mochihashi, and Y. Takashima, Phys. Rev. Lett. **118**, 094801 (2017).

[13] V. Epp and U. Guselnikova, Phys. Lett. A **383**, 2668 (2019).

[14] Y.-C. Lan, C.-H. Shen, and C.-M. Chen, Sci. Rep. **10**, 16768 (2020).

[15] F. Tamburini, B. Thidé, G. Molina-Terriza, and G. Anzolin, Nat. Phys. **7**, 195 (2011).

[16] P. L. Polavarapu, *Chiroptical Spectroscopy: Fundamentals and Applications* (Taylor & Francis, Boca Raton, 2017).

[17] Z.-Q. Zhang, J.-T. Lü, and J.-S. Wang, Phys. Rev. B **101**, 161406 (2020).

[18] Y.-M. Zhang and J.-S. Wang, J. Phys. Condens. Matter **33**, 055301 (2020).

[19] Z.-Q. Zhang and J.-S. Wang, Phys. Rev. B **104**, 085422 (2021).

[20] M. Ridley, L. Kantorovich, R. van Leeuwen, and R. Tuovinen, Phys. Rev. B **103**, 115439 (2021).

[21] Y.-M. Zhang, T. Zhu, Z.-Q. Zhang, and J.-S. Wang, Phys. Rev. B **105**, 205421 (2022).

[22] R. Berndt, R. Gaisch, J. Gimzewski, B. Reihl, R. Schlittler, W. Schneider, and M. Tschudy, Science **262**, 1425 (1993).

[23] X. Qiu, G. Nazin, and W. Ho, Science **299**, 542 (2003).

[24] Z. C. Dong, X. L. Zhang, H. Y. Gao, Y. Luo, C. Zhang, L. G. Chen, R. Zhang, X. Tao, Y. Zhang, J. L. Yang, and J. G. Hou, Nat. Photon. **4**, 50 (2010).

[25] E. Kazuma, J. Jung, H. Ueba, M. Trenary, and Y. Kim, Science **360**, 521 (2018).

[26] B. Doppagne, M. C. Chong, H. Bulou, A. Boeglin, F. Scheurer, and G. Schull, Science **361**, 251 (2018).

[27] Y. Zhang, Q.-S. Meng, L. Zhang, Y. Luo, Y.-J. Yu, B. Yang, Y. Zhang, R. Esteban, J. Aizpurua, Y. Luo, *et al.*, Nat. Commun. **8**, 15225 (2017).

[28] H. Imada, K. Miwa, M. Imai-Imada, S. Kawahara, K. Kimura, and Y. Kim, Nature **538**, 364 (2016).

[29] L. Zhang, Y.-J. Yu, L.-G. Chen, Y. Luo, B. Yang, F.-F. Kong, G. Chen, Y. Zhang, Q. Zhang, Y. Luo, *et al.*, Nat. Commun. **8**, 580 (2017).

[30] P. Merino, A. Rosławska, C. Große, C. C. Leon, K. Kuhnke, and K. Kern, Sci. Adv. **4**, eaap8349 (2018).

[31] C. C. Leon, A. Rosławska, A. Grewal, O. Gunnarsson, K. Kuhnke, and K. Kern, Sci. Adv. **5**, eaav4986 (2019).

[32] L.-L. Nian, Y. Wang, and J.-T. Lü, Nano Lett. **18**, 6826 (2018).

[33] L.-L. Nian, T. Wang, and J.-T. Lü, Nano Lett. **22**, 9418 (2022).

[34] D.-W. Zhang, M. Li, and C.-F. Chen, Chem. Soc. Rev. **49**, 1331 (2020).

[35] B. Göhler, V. Hamelbeck, T. Z. Markus, M. Kettner, G. F. Hanne, Z. Vager, R. Naaman, and H. Zacharias, Science **331**, 894 (2011).

[36] R. Naaman and D. H. Waldeck, J. Phys. Chem. Lett. **3**, 2178 (2012).

[37] S. Dalum and P. Hedegård, Nano Lett. **19**, 5253 (2019).

[38] R. Naaman, Y. Paltiel, and D. H. Waldeck, Acc. Chem. Res. **53**, 2659 (2020).

[39] Y. Liu, J. Xiao, J. Koo, and B. Yan, Nat. Mater. **20**, 638 (2021).

[40] F. Evers, A. Aharony, N. Bar-Gill, O. Entin-Wohlman, P. Hedegård, O. Hod, P. Jelinek, G. Kamieniarz, M. Lemeshko, K. Michaeli, V. Mujica, R. Naaman, Y. Paltiel, S. Refaely-Abramson, O. Tal, J. Thijssen, M. Thoss, J. M. van Ruitenbeek, L. Venkataraman, D. H. Waldeck, B. Yan, and L. Kronik, Adv. Mater. **34**, 2106629 (2022).

[41] S. Naskar, A. Saghatchi, V. Mujica, and C. Herrmann, Isr. J. Chem. **62**, e202200053 (2022).

[42] J. L. Greenfield, J. Wade, J. R. Brandt, X. Shi, T. J. Penfold, and M. J. Fuchter, Chem. Sci. **12**, 8589 (2021).

[43] L. Wan, Y. Liu, M. J. Fuchter, and B. Yan, Nat. Photon. **17**, 193 (2023).

[44] H. Haug, A.-P. Jauho, *et al.*, *Quantum kinetics in transport and optics of semiconductors*, Vol. 2 (Springer, 2008).

[45] M. Graf and P. Vogl, Phys. Rev. B **51**, 4940 (1995).

[46] A.-M. Guo and Q.-f. Sun, Phys. Rev. Lett. **108**, 218102 (2012).

[47] A.-M. Guo, E. Díaz, C. Gaul, R. Gutierrez, F. Domínguez-Adame, G. Cuniberti, and Q.-f. Sun, Phys. Rev. B **89**, 205434 (2014).

[48] J.-S. Wang, J. Peng, Z.-Q. Zhang, Y.-M. Zhang, and T. Zhu, arXiv preprint arXiv:2208.03511 (2022).

[49] K. Kaasbjerg and A. Nitzan, Phys. Rev. Lett. **114**, 126803 (2015).

[50] Z. Xie, T. Z. Markus, S. R. Cohen, Z. Vager, R. Gutierrez, and R. Naaman, Nano Lett. **11**, 4652 (2011).

[51] L. Xiang, J. L. Palma, Y. Li, V. Mujica, M. A. Ratner, and N. Tao, Nat. Commun. **8**, 14471 (2017).

[52] D.-S. Hu, C.-P. Zhu, L.-Q. Zhang, D.-R. He, and B.-H. Wang, Chin. Phys. Lett. **25**, 1822 (2008).